AIAA-92-0235

A Laminar Vortex Interacting With a Premixed Flame: Regimes of Interaction

Wm. L. Roberts and J. F. Driscoll
Department of Aerospace Engineering,
University of Michigan
Ann Arbor, Michigan

M. C. Drake
Physical Chemistry Department,
General Motors Research
Warren, Michigan

30th Aerospace Sciences
Meeting & Exhibit
January 6-9, 1992 / Reno, NV

A Laminar Vortex Interacting With a Premixed Flame:

Regimes of Interaction

Wm. L. Roberts* and J. F. Driscoll**
Department of Aerospace Engineering,
University of Michigan
Ann Arbor, MI 48109

and

M. C. Drake
Physical Chemistry Department,
General Motors Research
Warren, MI 48090-9055

Abstract

A single toroidal, laminar vortex interacts with a counterpropagating laminar premixed flame in order to study the fundamentals of the flame-vortex interaction. This flame-vortex interaction represents a fundamental "building block" of premixed turbulent combustion. Experimental results quantify the degree of flame rollup, the flame perimeter increase due to wrinkling, the boundary of the pocket formation (corrugated flame) regime and local quenching of the premixed flame. The measured trends indicate that viscous attenuation of the vortex by the hot, viscous products is important. Local quenching occurs at the leading edge of the vortex when the Karlovitz number (based upon the vortex diameter and rotational velocity) exceeds 0.1, which is significantly less than the value of unity predicted previously. Quenching is believed to result from a combination of flame stretch and radiative heat loss in the burnt gas. The importance of flame stretch is verified; as Lewis number is varied it is found that in order to form pockets, diffusionally stable flames require a vortex strength that is three time larger than that required by the diffusionally unstable flames. Effects of flame curvature are quantified; the highest OH intensities occur when the flamefront is convex towards the reactants, as expected for these flames for which Lewis number <1. The results are compared with the numerical solutions of the Navier-Stokes equations obtained by Poinsot, Veynante and Candel. These experiments help to quantify regimes for which the local flamelet approach is valid in the modeling of turbulent premixed flames.

Introduction

A flame-vortex interaction is shown schematically in Figure 1. Shown is a planar view of a toroidal vorticity layer. The rotational velocity of the vortex has two effects. First, there is a hydrodynamic effect caused by the vortex velocity field which wrinkles the flame and can cause pockets even with no stretch or viscosity effects. The vortex induces a velocity on centerline towards the flame, which retards flame motion on centerline; the vortex velocity far from centerline has a component in the direction of flame propagation, causing the flame to wrinkle as shown in Fig. 1. As this wrinkle passes over the rear portion of the vortex, the rotational velocity pulls the flame toward centerline which tends to create a pocket of unburned reactants if U_θ / S_L is sufficiently large. Secondly, the rotational velocity exerts stretch on the flame which can augment this wrinkling/pocket formation process. Flame stretch is due to the imposed strain field and to flame curvature. The stagnation point strain field near centerline induces positive stretch and can reduce the local burning velocity for Lewis numbers exceeding unity. The curvature of the flame at centerline induces negative stretch, which can affect the burning velocity in a manner opposite to the strain field. The flame curvature is similar to that of an inverted Bunsen burner, which is well documented [1]. Some vortex conditions for which strain dominates over curvature (and vice versa) were predicted by the numerical solutions of Poinsot et al. [8].

The present study is designed to address four important questions in turbulent premixed flames. First, the degree of strain, curvature and quenching exerted on a flame by each vortex in a turbulent flowfield is not known. There is abundant information about a steady, planar laminar flame

* Student Member
** Professor, Aero Eng
Member AIAA

in a strain field near a stagnation point [1,2]. However, the planar stagnation point flame properties may not adequately simulate local conditions near strained turbulent flames because turbulent vortices introduce the additional effects of flame curvature and a time varying strain field [3] as the vortex passes over the flame. The present study of a single vortex passing through a flame can be used to understand how planar stagnation point flames can be related to turbulent flames.

The second research question relates to the formation of pockets, or islands, of unburned reactants. The vortex strength required to form pockets and therefore cause the flame to enter the "corrugated flame" regime is not known. Examples of very wrinkled turbulent flamefronts are shown in Refs 4-7. These pockets of reactants may then quench the flamefront, allowing reactants to survive. This can cause excessive levels of carbon monoxide or unburned hydrocarbons which may account for combustion inefficiencies. The present results quantify the boundaries of the corrugated regime and the local extinction regime for a single vortex and allow for the assessment of two recent numerical simulation methods which predict the formation of pockets and flamefront quenching. Poinsot et al. [8] and Rutland et al. [9] solve the Navier Stokes equations numerically for a laminar flame-vortex interaction. Kwon et al. [10] and Wu et al. [4] use a flame interface simulation which also predicts the formation of pockets. These flame advection codes are unable to provide any information about reaction rate and thus are incapable of predicting quenching. Other simulations of the flame-vortex interaction have been reported by Chate and Cant [11] and Ashurst and McMurtry[12] and Peters and Williams [13]. Knowledge of where the boundaries are between these regions will permit modification to traditional turbulent combustion diagrams and determine where the local flamelet model is applicable and justified.

The third research question concerns the minimum diameter of vortices that can wrinkle a premixed flame. Peters [14] describes a minimum vortex diameter which he denotes the Gibson scale. Poinsot et al. [8] predict that a different vortex scale is the smallest that wrinkles the flame. That is, the minimum scale of wrinkling and the conditions at which pockets first form are strongly influenced by gas viscosity and flame curvature.

The fourth question is at what Karlovitz number quenching begins. The nondimensional Karlovitz number, defined as $(U_\theta/d_o)/(S_L^2/\alpha)$, is a measure of the flame stretch, which is composed of both flame strain and flame curvature effects. In traditional turbulent combustion diagrams, a Ka of unity is usually taken to be the border between the corrugated flame region and the distributed reaction zone region. In most numerical simulations, the border between pocket formation and quenching is assumed to asymptotically approach this limit of unity.

Apparatus

The experiment consists of a rectangular flame tube, 61 cm high and 11.4 cm on a side, as shown in Figure 2 [15,16]. The front is optical quality glass, and each side has a slit covered with glass for visualization experiments utilizing a laser sheet. For the hydroxal radical fluorescence images, non-fluorescing fused silica was used on the front and sides. The bottom of the flame tube contains a spark source and a fuel delivery tube. The top is sealed by either a 20.3 cm diameter or 10.2 cm diameter loudspeaker. Located 55.9 cm from the bottom of the flame tube is an interchangeable sharp-edged orifice plate. The orifice diameters range from 0.64 cm to 5.1 cm.

Experiments were conducted using either methane or propane at an equivalence ratio ϕ of 0.6. Equivalence ratio was maintained precisely through the use of critical flow orifices for both the fuel and air. The fuel and air are mixed externally and allowed to flow through the flame tube for a sufficient time to allow 5 volumes of the tube to be displaced, thus insuring adequate purging and an accurate equivalence ratio. The mixture is ignited using a standard automotive spark-plug. The hot products are exhausted during the interaction through solenoid operated ports (2.5 x 7.6 cm) near the bottom of the flame tube and pressure relief valves in the upper chamber. The pressure rise is thought to be on the order of 2 psi for equivalence ratios near 0.6.

The undisturbed laminar burning velocity of methane at ϕ of 0.6 was determined experimentally to be 8 cm/s. S_L was measured by subtracting the gas velocity ahead of the flame (34 cm/s), as measured using laser velocimetry, from the flame speed in laboratory coordinates (42 cm/s), determined from VCR images. After this measurement was made, the exhaust ports were doubled in size to reduce the pressure driving the flamefront, thus reducing the flame speed in laboratory coordinates to 14cm/s. The resulting value of 8cm/s is in general agreement with Yamaoka and Tsuji [17], Yu et al [18] and Lewis and Von Elbe [19]. Very smooth, non-wrinkled laminar flames were achieved for ϕ=0.6, but the flamefront became wrinkled due to thermo-diffusive instabilities in the methane, and hydrodynamic instabilities caused by the increased pressure (because of increased S_L) in the propane.

To generate a vortex ring, a voltage ramp function is applied across the coil of the loudspeaker, causing the speaker to deflect and push fluid through the orifice [20-23]. The translational velocity of the vortex core and the maximum rotational velocity were measured using laser velocimetry and were determined to be approximately equal. Both velocities were a function of the voltage applied to the speaker, the diameter of the orifice and the pulse duration of the voltage ramp function. Rotational velocities between 2.5 cm/s and 200 cm/s were achieved. The combinations of d_o (0.64 to 5.1 cm), U_θ and S_L (8 to 14 cm/sec) allowed Ka to vary from between 0.005 and 1.0

The rotational and translational components of the

vortex toroid were measured using a single component LDV system operated in the forward scattering mode in conjunction with micron sized oil droplet seeding and an Argon ion laser illumination . A commercial counter processor was used to produce an analog output relating voltage to velocity which was plotted as the vortex propagated over the probe volume.

Mie Scattering Tomography was used to visualize the flame-vortex interaction. Micron-sized oil drops from a TSI 9301 atomizer were added to the reactants and disappeared at the flame front. An argon ion laser and a cylindrical lens were used to form a laser sheet which was viewed using a LoCam II 16 mm camera operated at 300 frames/sec with a 10 nm interference filter to remove flame radiation.

The OH fluorescence was excited using a Nd:Yag-pumped dye laser, with frequency doubled output of 2 mJ at 282.7 nm [24.25] pumping the $Q_1(5)$ line of the (1,0) band of the $OH(X^2\Pi - A^2\Sigma+)$ transition. The laser light sheet used was 5.1 cm high and less than 200 micron thick. Single laser-shot images of a 50 mm x 68 mm region on the combustor centerline were detected using a cooled intensified CCD array camera having a 576 x 384 pixel array and a 14-bit A/D converter. All of the images were normalized to account for the spatial variation in the average laser power across the sheet and were corrected for a small noise background. Because single shot variations in laser power and laser frequency were not recorded, images with a section of undisturbed flamefront were normalized by the peak OH intensity in that region.

Results-Measured Vortex Velocity Field

Velocity profiles were measured using laser velocimetry to characterize the strength of each vortex used and to provide input conditions for numerical models. U_θ is defined as the maximum rotational velocity in the undisturbed vortex. Using conservation of momentum and mass relations [16], U_θ is predicted to be proportional to $(\Delta V)^2/t_r d_o^5$. The amount of fluid pushed through the orifice by the loudspeaker is ΔV, which is proportional to the voltage applied across the speaker coils; t_r is the time it takes this voltage to reach its final value; and d_o is the diameter of the orifice, all three of which are variables in this experiment. In addition, the analysis indicates that U_Z should be nearly equal to U_θ. A series of calibration curves were generated which relate the measured value of U_θ and U_Z to the operating parameter $(\Delta V)^2/t_r d_o^5$.

Figure 3 shows a typical vortex ring cross-section visualized by the laser light sheet. Oil drops were added only to the upper chamber in this case. These images were used to determine that the vortex core to core distance is 1.2 d_o at this downstream location, where d_o is the orifice diameter, which is consistent with previous vortex studies [17].

$U_{Z,max}$ was defined as the maximum value of the profile of U_Z versus time generated from the analog output from the LDV system. At each y location, a value of $U_{Z,max}$ was determined and is plotted in the lower curve of Figure 4. The lower curve in Fig. 4 is the axial velocity along the y axis, i.e. along the line drawn between the vortex cores. On centerline (y=0), $U_{Z,max}$ is about 130 cm/s due to the superposition of induced velocities from each of the core sections shown in Fig. 4. At y=1.5 cm, $U_{Z,max}$ reaches a maximum where the rotational velocity about the core is maximum. At y=2.2 cm, $U_{Z,max}$ has decreased to a local minimum of 20 cm/s, which is the sum of the positive translational velocity of the core (100 cm/s) and the negative rotational velocity. The core is defined as the location halfway between the maximum value of $U_{Z,max}$ at y=1.5 cm and the local minimum at y=2.2 cm.

The quantity U_θ is defined as the maximum rotational velocity within the vortex and was determined as follows. The maximum value of a profile of U_Y versus time is defined as $U_{Y,max}$. $U_{Y,max}$ is plotted as a function of y in the upper plot of Figure 4. At the core location, the value of $U_{Y,max}$ is due only to rotation, and thus U_θ is defined as $U_{Y,max}$ at the core location ($y=y_c$, as determined above). Figure 5 is a plot of the core translational velocity $U_{Z,C}$ and U_θ as a function of the experiment parameters. This figure shows that as speaker voltage ramp time t_r is varied, both U_θ and U_Z are directly proportional to $(\Delta V)^2/t_r d_o^5$, as predicted by conservation of momentum concepts. However, as ΔV and d_o are varied, the agreement with analysis is not as good as shown in Figure 5. In all cases, however, the rotational and translational velocities are nearly equal, within experimental error.

Results - Visualization of Flame-Vortex Interactions

The interaction between the laminar premixed flame and the laminar vortex ring can be characterized using four distinct classifications which are denoted the no effect regime, the wrinkled flame regime, the pocket formation regime, and the local extinction regime. The criterion for each regime is as follows. With no vortex present, the flame has a positive curvature due to wall boundary layers as shown in Fig. 2. In the no effect regime, the flame curvature remains positive. It was decided to denote the onset of wrinkling as the condition when the flame curvature becomes negative, i.e. concave on centerline. The pocket formation regime occurs if an independent pocket of reactants survives the flame passage for more than 1/60 of a second (one half-frame of the Mie scattering using a VCR). The local extinction regime is determined from the OH fluorescence images. The observed OH fluorescence is due entirely to superequilibrium OH in the reaction zone, because there is negligible OH signal from the burnt gas, as established from the images and the CHEMKIN code [26]. Therefore, the OH fluorescence signal is a good indicator of the reaction zone in lean premixed flames and the intensity of the signal is proportional to the reaction rate. Local

extinction is said to occur if the superequilibrium OH concentration decreases to less than one tenth of the unstretched value.

Figure 6 shows a very weak vortex (U_θ/S_L=0.5, Ka=0.005) interacting with the flame front. Reactants are on top of the interface and products are on the bottom, products appear black due to the lack of oil drops which burn up in the flame front. The cores of the vortex pair are also black because oil drops were not added to the upper chamber, so as to visualize the vortex core location. As can be seen, the vortex does not wrinkle the flame front. The flame forces the vortex cores to move apart in Fig. 6, which is similar to motions which occur when a vortex pair approaches a solid boundary. The parabolic shape of the flame surface also may help to separate the vortex cores.

In Figure 7 the vortex strength has been increased to U_θ/S_L=2.75 with a corresponding Ka=0.03. The vortex already is strong enough to separate itself from the flame front and exist as a pocket of reactants. This pocket completely disappears 131 ms after any effect on the flame by the vortex is first detected. The oil droplet visualization technique cannot identify whether the border between reactants and products is a reaction zone or is locally quenched. Note that there is very little "vortex wake" in Fig. 7. Combustion continues until all the reactants in the pockets are consumed.

In Figure 8 the vortex strength has been increased to U_θ/S_L=8.8 with Ka=0.95. The rotational velocity first pulls the flame in the vortex wake toward centerline, which creates a narrow necking of the reactants in the wake region. The flame then enters the rear of the vortex and begins to roll up. The wake is longer than in the previous figure due to the increased translational velocity (which is proportional to rotational velocity). The flame rolls up and travels almost 270 degrees around the vortex, causing the thin black interior lines observed in Fig. 8. A jet of hot gas products is observed to issue upward along the centerline in Figs. 8g-8i due to product expansion. The hot, viscous jet exiting the rear of the vortex tends to unroll the vortex, as evidenced by the white fingers of unburned reactants that extend nearly parallel to the wake.

Flame quenching is observed when the vortex strength is increased further (U_θ/S_L = 10.2, Ka=0.11) as seen in Figure 9. The flame rolls up in the vortex (Fig. 9a and 9b) and forms a pocket (Fig. 9c). However, the flame does not continue to spiral inward towards the core, as predicted by the constant density simulation of Peters and Williams [13]. Instead, hot products expand and are jettisoned out the rear of the vortex, causing the S-shaped pocket in Fig. 9d. This is similar to that observed with the Mie scattering in Figs. 8g-8i. The bottom part of Figure 9d also shows that the flame is nearly quenched at the leading edge of the vortex. Complete quenching is observed in Figs. 9e and 9f where reactions at the rear of the pocket continues but reactions have ceased at the leading edge of the vortex where the strain is largest. This is shown more quantitatively by the profiles of OH intensities in Fig. 10. The peak OH intensities of the trailing edges remain nearly constant, while the intensities in the leading edge decline rapidly from Fig. 9c to 9d and are essentially zero within our experimental error in Figs. 9e and 9f. Later images of the unburned gas pockets show a declining OH intensity around the pocket. These pockets may not burn completely and could be one source of hydrocarbon and CO emissions in lean-burn engine exhausts. These results are qualitatively the same as the full Navier-Stokes calculations for a flame-vortex interaction calculated by Poinsot et al.[8] which also shows pocket formation, leading edge quenching, and escape of unburned reactants. The Navier-Stokes calculations [8] and detailed chemistry calculations of stretched laminar single flames show this abrupt extinction process can not be caused by flame stretch effects alone and instead result from the combined effect of flame stretch and heat loss in the burnt gas. Quantitative model-experiment comparisons are not possible until the temperature field in the burnt gas and the velocity field ahead of the vortex are measured.

Regimes of Wrinkling, Pocket Formation and Quenching

The boundaries of the wrinkled flame regime and the pocket formation regime are plotted in Figures 11 and 12. For each Mie scattering data point plotted, 3-5 visualizations were recorded by the VCR camera; repeatability was excellent. Classical theory of flame wrinkling by Damkohler and by Shchelkin [19] predicts that the fractional increase in flame area should be only a function of normalized velocity fluctuations (U_θ/S_L in this case) and should not depend on vortex size. These classical concepts predict that a curve defining the degree of wrinkling would be a horizontal line in Fig 11. Instead, the boundaries between regimes in Fig. 11 have a negative slope.

The negative slope of the boundaries in Fig. 11 indicates that smaller vortices are less effective in wrinkling the flame and forming pockets than larger vortices of the same rotational velocity. Numerical simulations of Poinsot et al [8] have predicted that the regime boundaries should have negative slope, which agrees with the present results. Smaller vortices decay more rapidly than larger vorticies during flame passage because smaller vorticies have lower Reynolds number, ie., relatively larger viscous forces. In addition, smaller vortices create larger local flame curvature which can oppose wrinkling and pocket formation due to flame stretch.

Stretch, Curvature, and Lewis Number Effects

The Lewis number was varied so as to study both thermo-diffusively unstable flames (methane-air, ϕ = 0.6, Le = 1.02 [28]) and thermo-diffusively stable flames (propane-air, ϕ = 0.6, Le = 1.87). The unstable flames remained

smooth and non-cellular (see Figs. 6a, 7a, 8a) for $\phi < 0.7$ apparently because the hydrodynamic forces associated with non-uniform gas expansion were not strong enough to trigger the wrinkling. For $0.7 < \phi < 1.0$, the methane-air flames were cellular, as expected, and not appropriate for this type of study.

The flame regime boundaries for the diffusively unstable case (Fig. 11) and stable case (Fig 12) have similar negative slopes. However the vortex strengths U_θ/S_L required to form pockets in the diffusionally stable case are three times larger than the corresponding values for the unstable case. These findings indicate that flame stretch plays a significant role in the present interactions. In turbulent premixed flames, both Wu et al. [4] and Kwon et al. [10] report that preferential diffusion/flame stretch effects cause significant changes in the flame structure and the reactant consumption rates.

Local extinction was observed for the present methane-air flames but was not observed for the propane-air flames; the global extinction limit is plotted in Fig. 11. The strain rates and Karlovitz numbers stated are global values, and are not based on local instantaneous strain rates or curvature. For the flame-vortex interactions studied here, local quenching is observed for a global $Ka > 0.1$, considerably lower than the value of 1 often assumed. However, the value of 0.1 may not be a universal quenching limit for all flame-vortex interactions, and we anticipate it will vary with laminar burning velocity, heat loss rate, vortex size and strength, and flame-vortex interaction time.

In addition to quenching, flame curvature effects are also observed for these Le less than 1 flames. When the flame is convex towards the reactants, as in the two red peninsulas in Fig. 9d, the OH intensities (and by implication the reaction rates) are high. When the flame is convex towards the products, as in the top and sides of Fig. 9d, the OH intensities are lower. The peak OH intensities vary by a factor of 4 due to flame curvature effects. These observations are consistent qualitatively with stretched flame analysis [1].

While the present results confirm certain trends predicted by Poinsot et al., it is important to keep in mind several differences between their assumptions and the present experiment. The present vortex is an axisymetric toroid, whereas the numerical study considers a two dimensional pair of line vortices. The numerical study includes no vortex translational velocity or buoyancy forces which exist in the experiment. Realistic turbulent eddies will have translational velocities induced by neighboring vortices, as governed by the law of Biot and Savart [12]. The translational velocity enhances the flame wrinkling but does not, by itself, cause pockets to form. The numerical study also assumed a 1-step reaction rate and large radiative heat losses in the burnt gas, which may not correspond to our experimental conditions.

Peters and Williams [13] have simulated the interaction of a flame with a "frozen" vortex having a velocity field that is not disturbed by the flame. For several reasons, the flame in the present experiment does not roll up and undergo 3-5 revolutions about the vortex core, as predicted by Peters and Williams. The potential vortex in the analysis had rotational velocities that approach an infinite magnitude near the core; the present vortex has nearly zero rotational velocity at the core center. The maximum rotational velocity in the experiment was limited by transition to turbulence. Also, the large value of viscosity of the products and the expansion of gases that exit the vortex tend to reduce the rotational velocity; neither are considered in the constant density analysis of Peters and Williams.

The perimeter of the flame interface that is imaged in Figs. 6-9 is important because it helps to quantify the increase in reaction surface area caused by a single turbulent eddy. In Figure 13 time is normalized by d_o/S_L and the measured perimeter is normalized by the unperturbed perimeter. The upper curve corresponds to an interaction in the pocket formation regime (U_θ/S_L=8.8), while the lower curve corresponds to an interaction at the border between the wrinkled flame regime and the pocket formation regime (U_θ/S_L=2.75). Some negative values arise because the flame front is initially convex and flattens out, thus reducing the perimeter. Chate and Cant [11] have calculated the flame perimeter increase for a frozen vortex velocity field and have measured trends that are similar to those shown in Fig. 13.

Conclusions

1) Four distinct regimes of the flame-vortex interaction are observed; the no effect regime, the wrinkled flame regime, the pocket formation regime and the global quenching regime. Boundaries between these regimes were measured.
2) Smaller vortices are less likely to disturb the flame front than larger vortices having the same vortex strength (U_θ/S_L). These observations are consistent with the Navier-Stokes simulations of Poinsot et al. Smaller vortices have a lower Reynolds number than the larger vortices and thus decay due to viscous forces before they can effectively form pockets. Smaller vortices also cause larger flame curvature, which can prevent wrinkling. Using the present results, it can be estimated that a large fraction of the smaller vortices ahead of a typical turbulent flame are too weak to wrinkle the flame.
3) The global Karlovitz number $(Uq/do)/(S_L^2/\alpha)$ at which quenching occurs is 0.1 for the particular vortex diameter chosen; this value is significantly less than the value of unity estimated in previous analyses.
4) Stretch effects play an important role in the formation of reactant pockets, as evidenced by large effects of Lewis number on the results. Reaction rate is enhanced due to flame curvature when the flamefront is convex towards the reactants for these Le less than 1

flames, in agreement with stretched laminar flame theory.

5) The translational velocity of the vortex with respect to the reactants (Uz) is important in the flame wrinkling and pocket formation processes. U_Z must be included for accurate numerical simulations of this experiment as well as general turbulent flows. Due to U_Z, cusps were formed in the flame surface which point toward the products, which are commonly observed in turbulent flames.

6) The increase in flame front perimeter was quantified during the flame wrinkling and pocket formation processes.

7) The present results, particularly when coupled with direct numerical simulations, will help define the limits of stretched laminar flamelet models in turbulent combustion.

References

1. Law, C.K., Twenty-Second Symposium (International) on Combustion, The Combustion Institute, Pittsburgh, 1988, pp. 1381-1402.
2. Darabiha, N., Candel, S.M., Giovangigli, V. and Smooke, M.D., Combust. Sci. Technol. 60, 267 (1988).
3. Haworth, D.C, Drake, M.C, Pope, S.B. and Blint, R.J., Twenty-Second Symposium (International) on Combustion, The Combustion Institute, Pittsburgh, 1988, pp. 589-597.
4. Kwon, S., Wu, M.S., Driscoll, J.F. and Faeth, G.M., Combust. Flame, to appear.
5. Mantzeras, J., Felton, P.G., and Bracco, F.V., Combust. Flame 77, 295 (1989).
6. Murayama, M. and Takeno, T., Twenty-Second Symp. (International) on Combustion, p. 551 (1988).
7. Becker, H., Monkhouse, P.B., Wolfrum, J., Cant, R.S., Bray, K.N.C., Maly, R., Pfister, W., Stahl, G., and Warnatz, J., Twenty-Third Symp. (International) on Combustion, p. 817 (1990).
8. Poinsot, T., Veynante, D., and Candel, S., Twenty-Third Symposium (International) on Combustion, The Combustion Institute, Pittsburgh, 1990, to appear.
9. Rutland, C.J., Ferzinger, J.H., and El Tahry, S.H., Twenty-Third Symposium (International) on Combustion, The Combustion Institute, Pittsburgh, 1990, to appear.
10. Wu, M.S., Kwon, D., Driscoll, J.F. and Faeth, G.M., Combust. Sci. Technol. 78:69 (1991).
11. Chate, H. and Cant, R.S., Combust. Flame 74: 1-8 (1988).
12. Ashurst, W.T. and McMurtry, P.A., Combust. Sci. Technol. 66: 17-38 (1989).
13. Peters, N. and Williams, F.A., Twenty-Second Symposium (International) on Combustion, The Combustion Institute, Pittsburgh, 1988, pp. 495-503.
14. Peters, N., Twenty-First Symposium (International) on Combustion, The Combustion Institute, Pittsburgh , 1986, pp. 1231-1250.
15. Roberts, W.L. and Driscoll, J.F., accepted for publication in Combust. Flame, (1991).
16. Roberts, W.L., Driscoll, J.F., Drake, M.C., and Ratteliff, J.W., submitted for publication in Twenty-Fourth Symposium (International) on Combustion, The Combustion Institute, Pittsburgh
17. Yamaoka, I. and Tsuji, H., Twentieth Symposium (International) on Combustion, The Combustion Institute, Pittsburgh, 1984, pp. 1883-1892.
18. Yu, G., Law, C.K., and Wu, C.K., Combust. Flame 63: 339-347 (1986).
19. Lewis, B. and von Elbe, G. Combustion, Flames and Explosions of Gases, Academic Press, 1961.
20. Jarosinski, J., Lee, J.H.S., and Knystautas, R., Twenty-Second Symposium (International) on Combustion, The Combustion Institute, Pittsburgh, 1988, pp. 505-514.
21. Maxworthy, T., J. Fluid Mech. 51: 15-32 (1972).
22. Dahm, W.J.A., Scheil, C.M., Tryggvason, G., J. Fluid Mech. 205: 1-43 (1989).
23. Macgarvey, R.H. and MacLatchy, C.S., Can. J. Phys. 42: 678-683 (1963).
24. Drake, M.C. and Pitz, R.W., Experiments in Fluids 3, 283, (1985).
25. Kychakoff, G., Howe, R.D., Hanson, R.K., Drake, M.C., Pitz, R.W., Lapp, M. and Penney, C.M., Science 224, 382 (1984).
26. Kee, R.J., Grear, J.F., Smooke, M.D., and Miller, J.A., Sandia Technical Report SAND 85-8240, Sandia National Laboratories, Livermore, CA (1985).
27. Drake, M.C. and Blint, R.J., Combust. Sci. Technol. 75, 261 (1991).
28. Mizomoto, M., and Yoshida, H., Combust. Flame 70: 47-60 (197).

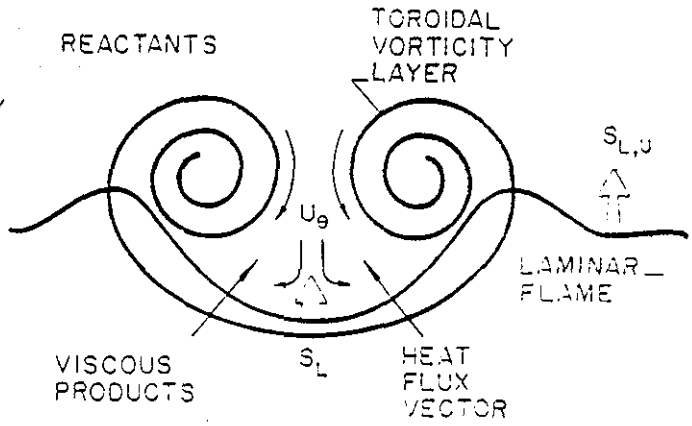

Figure 1 Schematic of Laminar Flame Propagating Upward Over Toroidal Vortex. On centerline, flame experiences positive strain (similar to stagnation point flows) which decrease S_L and negative curvature (similar to an inverted Bunsen burner) which increases S_L for Le>1.

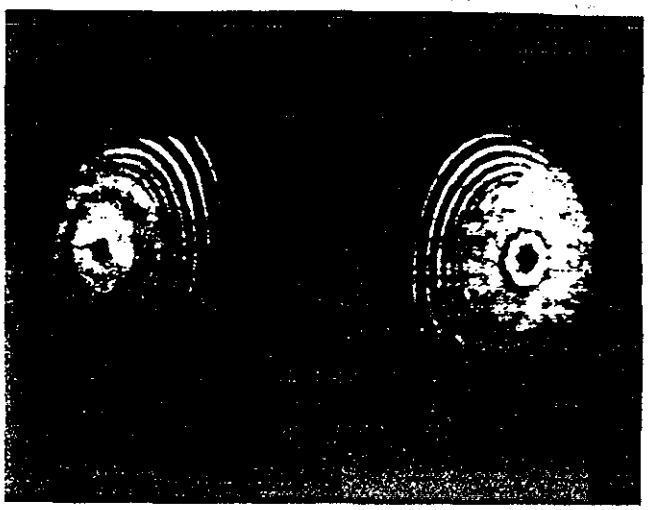

Figure 3 A Typical Undisturbed Vortex Ring Photographed Using a Laser Light Sheet and Submicron Oil Drops

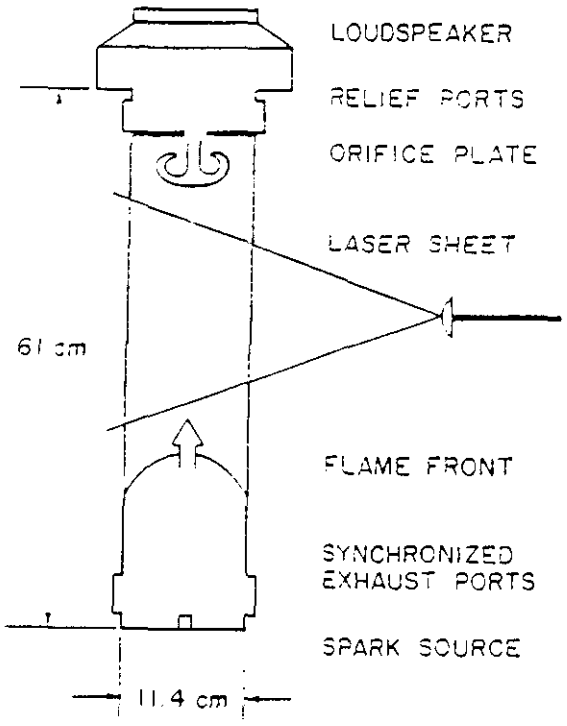

Figure 2 Apparatus Used to Interact Laminar Flame and Laminar Vortex

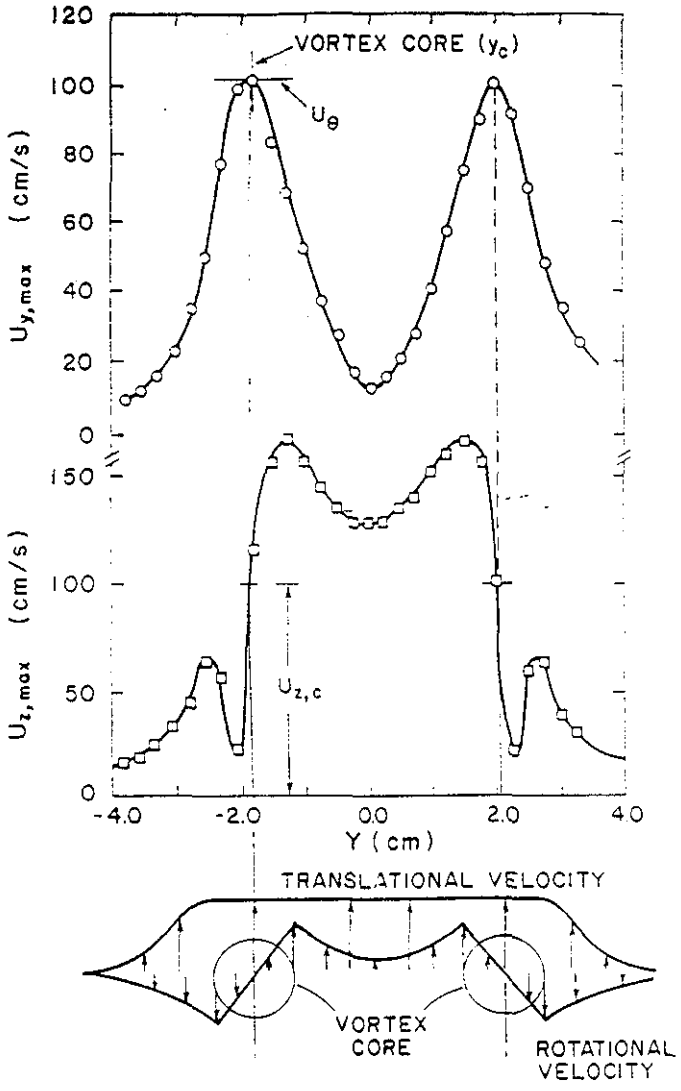

Figure 4 Radial Variation of $U_{y,max}$ and $U_{Z,max}$ Used to Determine Core Location, Maximum Rotational Velocity U_θ, and Axial Velocity of Core $U_{Z,C}$ from Laser Velocimeter Data. U_θ=100cm/s, d_O=3.81cm.

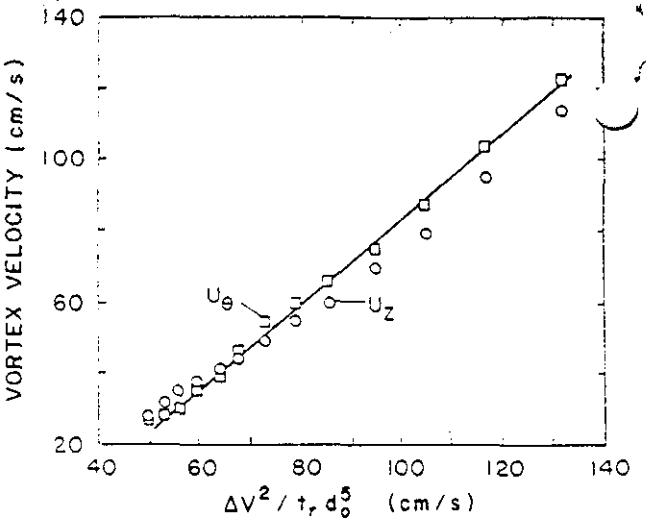

Figure 5 Measured Maximum Rotational Velocity (U_θ) of Vortex and Axial Velocity of Core ($U_{Z,C}$) For a Given Loudspeaker Volume Displacement (ΔV), Voltage Ramp-up Time (t_r), and Orifice Diameter (d_O).

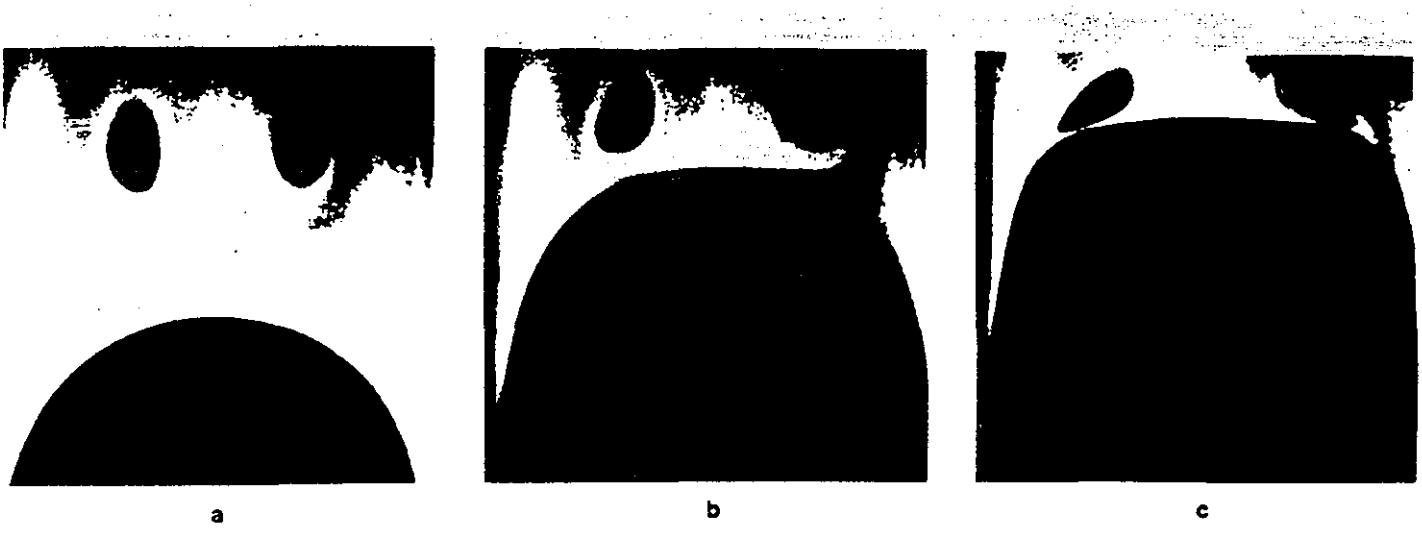

Figure 6 A Weak Vortex (U_θ/S_L=0.5, d_O/δ_F=37.2, Ka=0.005) That Has No Effect on Flame Front. The distance between vortex cores increases, similar to vortices interacting with a solid surface. Methane, ϕ=0.6

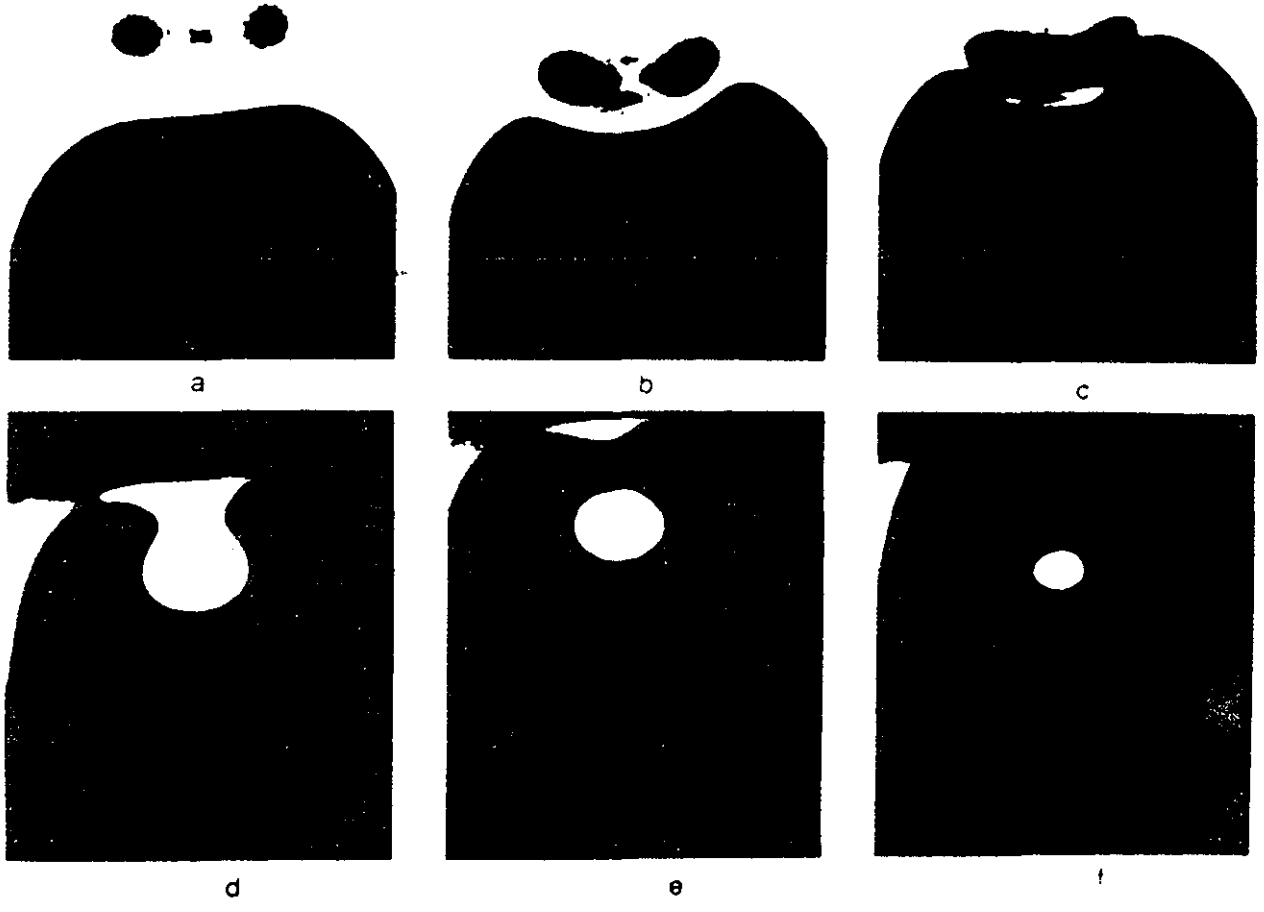

Figure 7 Formation of Pocket of Reactant with No Flame Rollup. U_θ/S_L=2.75, d_O/δ_F=37.2, Ka= 0.03, methane, ϕ=0.6, time: a: 31ms, b: 63ms, c: 77ms, d: 100ms, e: 106ms, f: 111ms

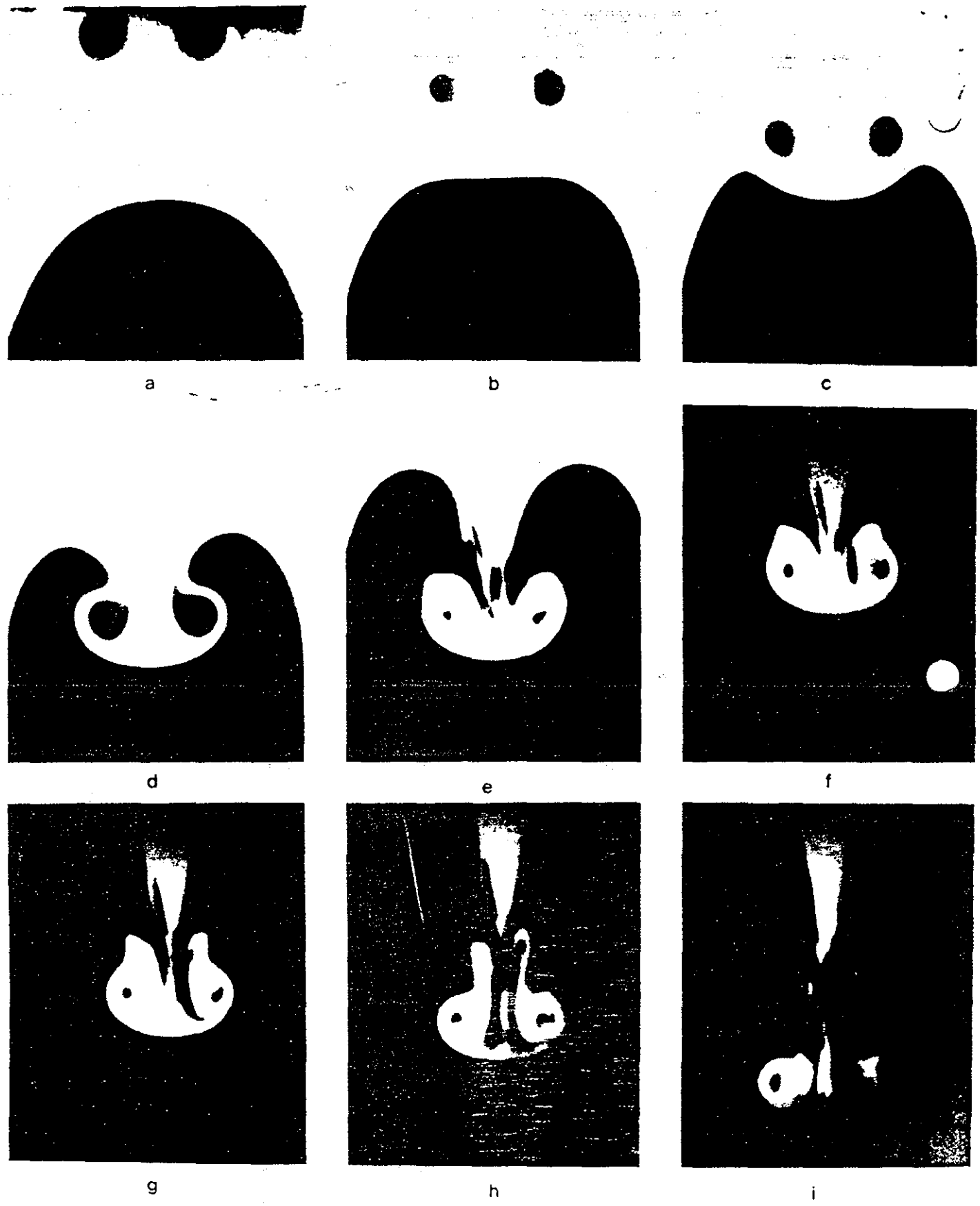

Figure 8 Formation of Pocket of Reactants with Flame Rollup. U_θ/S_L=8.8, d_O/δ_F=37.2, Ka= 0.95, methane, ϕ=0.6, time: a: -11.4ms, b: 8.6ms, c: 23ms, d: 34.3ms, e: 57ms, f: 66ms, g: 71.4ms, h: 77ms, i: 83ms.

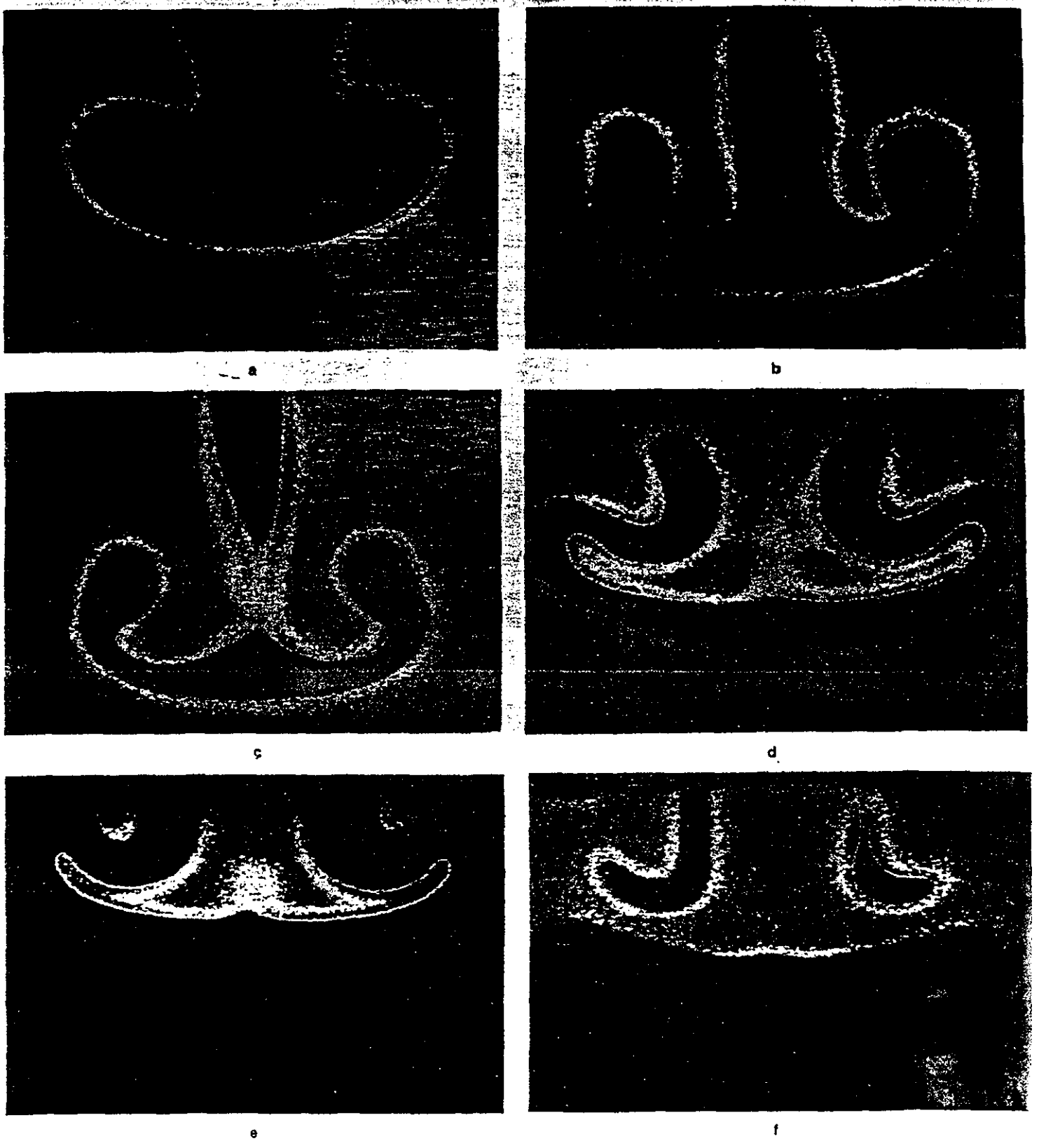

Figure 9 Quenching of the Flame Near the Vortex Leading Edge. Strong vortex case (U_θ/S_L=10.2, Ka= 0.11, d_O/δ_F=37.2) OH fluorescence from lower boundary of the pocket in image (d) no longer appears in images (e) and (f). Flame does not consume the reactants. Methane-air, ϕ = 0.6. Approximate time from initial interaction: a = 40ms; b = 60ms; c = 75ms; d = 100ms; e = 110ms; f = 115ms. Relative OH intensity: red = 0.5-1.0; yellow = 0.3-0.5; green = 0.2-0.3; blue = 0.1-0.2; black = below 0.1.

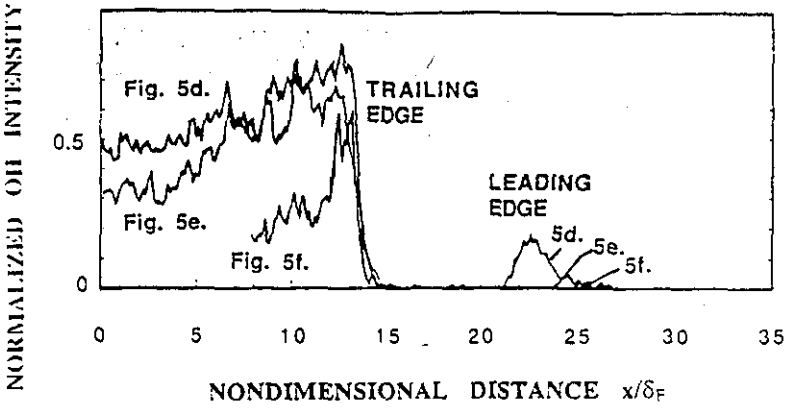

Figure 10 Profiles of Centerline OH Intensity Across the Flames in Figs. 9d, e, and f.

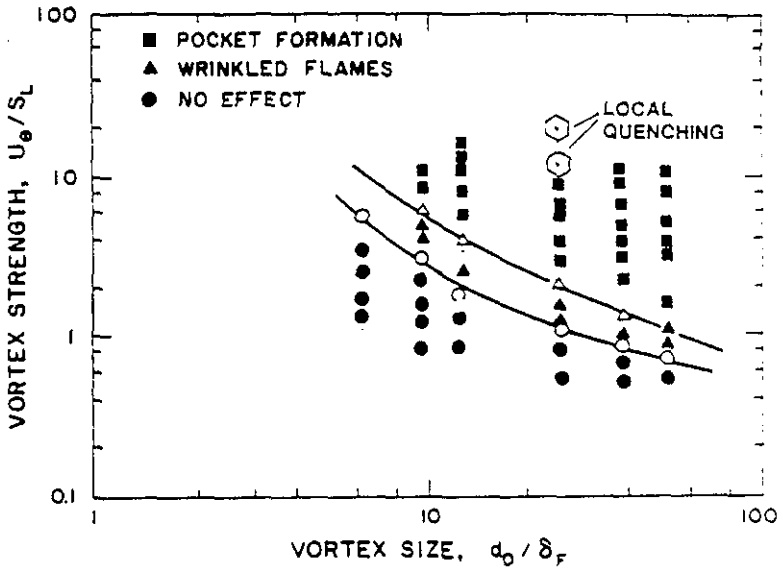

Figure 11 Regimes of Wrinkled Flames, Pocket Formation (Corrugated Flames) and Local Quenching Measured For Diffusionally Unstable Conditions. Methane, ϕ=0.6. Negative slope of boundaries is attributed to viscosity and flame curvature effects, as shown by numerical simulation of Poinsot, et al.

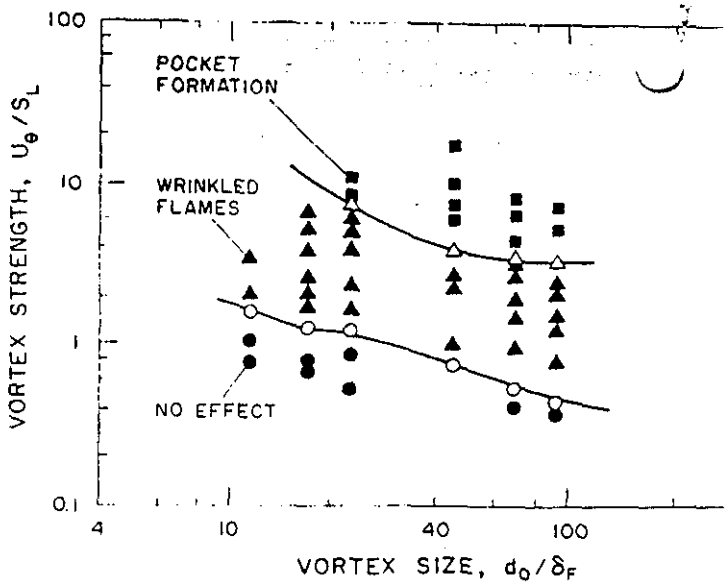

Figure 12 Regimes of Wrinkled Flames and Pocket Formation (Corrugated Flames) Measured For Diffusionally Stable Conditions. Propane, ϕ=0.6, Le=1.87. Note that to form pockets, vortex strength must be three times larger for the above stable conditions than for unstable conditions (Fig. 11). Also, no quenching is observed.

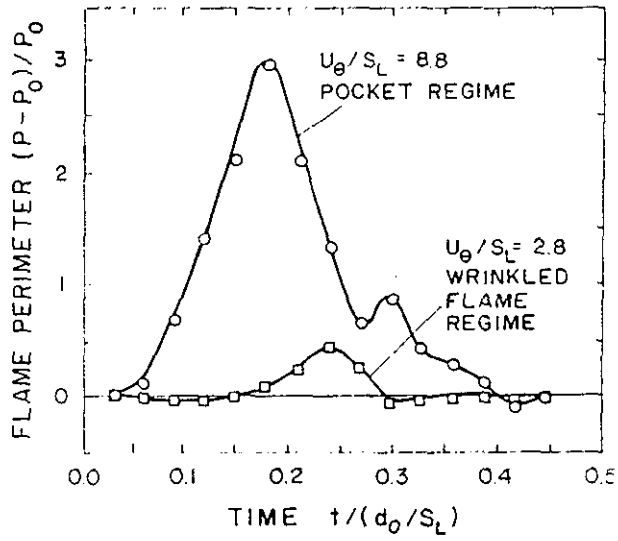

Figure 13 Measured Perimeter of Laser Light Sheet Image of Flame Surface. P_O is perimeter of undisturbed flame : $U\theta/S_L$=8.8, : $U\theta/S_L$=2.75, d_O=3.81 cm, S_L=8 cm/s, methane, ϕ=0.6. Some predicted flame perimeters are given Chate and Cant [7].